Virology 417 (2011) 281–292

Contents lists available at ScienceDirect

Virology

journal homepage: www.elsevier.com/locate/yviro

Osteopontin upregulation in rotavirus-induced murine biliary atresia requires replicating virus but is not necessary for development of biliary atresia

Paula M. Hertel [a,*], Sue E. Crawford [b], Milton J. Finegold [a,c], Mary K. Estes [b]

[a] Department of Pediatrics, Baylor College of Medicine, Houston, TX 77030, USA
[b] Department of Molecular Virology and Microbiology, Baylor College of Medicine, Houston, TX 77030, USA
[c] Department of Pathology, Baylor College of Medicine, Houston, TX 77030, USA

ARTICLE INFO

Article history:
Received 30 November 2010
Accepted 26 May 2011
Available online 13 July 2011

Keywords:
Rotavirus
Biliary atresia
Osteopontin
Antigenemia
Fibrosis
Cholestasis
Pediatrics
Liver
Bile ducts

ABSTRACT

Biliary atresia (BA) is a progressive fibro-inflammatory pediatric liver disease in which osteopontin (OPN), a glycoprotein with inflammatory and fibrogenic activity, may play a pathogenic role. The current studies were conducted in a mouse model of rotavirus-induced BA to test the hypotheses that live but not inactivated rotavirus causes antigenemia, upregulation of hepatic OPN expression, and induction of BA and fibrosis; and that OPN is necessary for development of BA. Prolonged or transient antigenemia developed in mice inoculated with live or inactivated virus, respectively, but only live virus upregulated hepatic OPN and caused BA and fibrosis. OPN was expressed in intra- and extrahepatic bile ducts in healthy mice and in mice with BA. OPN-deficient mice, similar to WT mice, developed BA. Together, these data show that live but not inactivated rotavirus causes upregulation of hepatic OPN expression and BA but that OPN is not necessary for development of BA.

Introduction

Biliary atresia (BA) is a serious childhood liver disease in which fibro-inflammatory obliteration of bile ducts results in progressive liver damage. Fibrogenesis is notably rapid, and some infants develop cirrhosis within months of disease onset. BA represents the most common indication for liver transplant in children (Sokol et al., 2007). In approximately 85% of cases, there are no other organ anomalies and infants are born apparently healthy, but jaundice and onset of progressive liver disease occur within the first several weeks of life. The cause of this "perinatal" form of biliary atresia is unknown, but it has been hypothesized that viral infection may provide an initial insult that triggers immune-mediated damage to intra- and extrahepatic bile ducts that persists even after viral infection has cleared (Mack et al., 2005, 2006; Shivakumar et al., 2004).

Although data are contradictory, a number of viruses, including cytomegalovirus, Epstein-Barr virus, reovirus type 3, human papillomavirus, human herpesvirus 6, and group C rotavirus, have been implicated as potential etiopathogenic agents of perinatal biliary atresia (Domiati-Saad et al., 2000; Drut et al., 2008; Qiao et al., 1999; Mahjoub et al., 2008; Tyler et al., 1998). In one series, group C rotavirus RNA was identified in 10 of 20 patients diagnosed with biliary atresia or choledochal cyst, whereas none of 12 similarly-aged controls with other types of liver disease had detectable rotavirus in their livers (Riepenhoff-Talty et al., 1996).

Identification of rotavirus in the liver tissues of BA patients indicates a possible association between virus infection and BA, and a well-established mouse model of rotavirus-induced BA serves as evidence that a viral infection can initiate an inflammatory response that leads to BA (Allen et al., 2007; Mack et al., 2005, 2006; Nadler et al., 2009; Petersen et al., 1997; Riepenhoff-Talty et al., 1993; Shivakumar et al., 2004). In this model, neonatal mice inoculated intraperitoneally (ip) with rhesus rotavirus (RV) develop infection of biliary epithelium followed by a Th1-biased, immune-mediated bile duct damage resulting in progressive liver disease. The clinical disease and histopathological findings in the murine BA model closely resemble BA in human infants. Replicating virus has been identified in liver homogenates from RV-infected mice with BA, but there are no published studies that use immunohistochemistry to identify nonstructural viral components (such as NSP4, the presence of which indicates viral replication) in bile ducts. The presence of RV in the blood, or antigenemia, also requires study in the BA mouse model. RV antigenemia is a phenomenon that has recently been demonstrated in normal RV-infected mouse and human hosts (Blutt et al., 2006, 2007). There are no published reports, however, investigating RV serum antigenemia in the BA mouse model (or, for that matter, in mouse pups inoculated at the young age of 2 days old or via the ip route).

* Corresponding author at: Department of Pediatrics, Baylor College of Medicine, One Baylor Plaza, Houston, TX 77030, USA. Fax: +1 832 825 3633.
E-mail address: phertel@bcm.edu (P.M. Hertel).

0042-6822/$ – see front matter © 2011 Elsevier Inc. All rights reserved.
doi:10.1016/j.virol.2011.05.015

Osteopontin (OPN) is a multifunctional glycoprotein that can induce Th1 cytokine activity and promote fibrogenesis, both of which may play an important role in the pathogenesis of human BA (Cantor and Shinohara, 2009; Harada et al., 2003; Syn et al., 2010; Szalay et al., 2009; Vetrone et al., 2009). A microarray study showed that osteopontin mRNA expression was upregulated in liver biopsy specimens from human BA patients (Bezerra et al., 2002). OPN protein is expressed in the intrahepatic bile ducts of BA patients but not in those of healthy children, with the intensity of osteopontin staining correlating with severity of fibrosis (Huang et al., 2008; Whitington et al., 2005). These findings suggest that pathogenic mechanisms unique to BA, which distinguish BA from certain other childhood liver diseases, may include biliary upregulation of OPN expression.

Hepatic OPN expression was shown to be increased in a mouse model of nonalcoholic steatohepatitis, and OPN-deficient mice had reduced inflammation and fibrosis compared with WT mice in this model (Sahai et al., 2004). OPN expression levels and patterns in the mouse BA model have not been reported. A microarray study of the rotavirus BA model did not report up- or down-regulation of OPN in extrahepatic biliary tissues, but liver tissue was not examined in that study (Carvalho et al., 2005). Here, we report use of the RV BA mouse model and *in vitro* studies to determine if OPN expression is increased in the liver in BA, if OPN contributes to development of BA, and if replicating RV is required to elicit antigenemia, OPN expression, and BA.

Results

Induction of BA in neonatal mice requires high doses of replicating RV

To set up the mouse model of RV-induced biliary atresia, we intraperitoneally inoculated neonatal mice (24–48 h after birth) with purified triple-layered rhesus RV particles. The amount of virus necessary to cause BA in 50% of the mice (the BA_{50}) was determined to be 4.8×10^6 plaque forming units (pfu). This dose was significantly higher than the dose determined to cause an antibody response in 50% of the animals (the ID_{50}), which was 553 pfu. The antibody responses in these animals resulted from infection rather than from the ip-injected viral antigenic load based on control experiments that evaluated the geometric mean antibody titer (GMT) of pups given equivalent high amounts (4×10^7 pfu) of purified live and inactivated virus and found a 32-fold higher titer in animals given live virus. The GMT at the ID_{50} was ~9, so, extrapolating from the data above, it would be expected that no antibody would be detected in animals given the equivalent of the ID_{50} of inactivated virus.

To maximize the possibility of inducing BA with inactivated RV, a high inoculation dose of 8.3 BA_{50} doses (4×10^7 pfu or 7.9×10^4 ID_{50} doses) was used in subsequent experiments that evaluated the time course of development of BA, the requirement for replicating virus to induce BA, and the effect of RV on OPN expression.

Following inoculation with either live or inactivated purified RV, BA development was assessed in neonatal mice at 4 days post-inoculation (dpi), 9–10 dpi, or at 15–16 dpi. At 4 dpi, three of seven pups inoculated with live RV had acholic stools and bilirubinuria, and no extrahepatic bile duct abnormalities were visualized. All pups (N = 5) inoculated with live virus and assessed at 9–10 dpi had developed BA (Fig. 1), and 9 of 10 had BA at 15–16 dpi. The live virus-inoculated pup that did not meet BA criteria at 15–16 dpi had previously appeared sickly and jaundiced like its littermates, so this pup presumably developed BA and then recovered. By 15–16 dpi, all pups inoculated with live virus with BA were visibly stunted, oily, jaundiced, and physically inactive compared with inactivated virus and saline treated animals, which were all robust, pink, and, physically active (Fig. 2a). No pups inoculated with inactivated virus (N = 24) or with saline (N = 14) exhibited any of the criteria for BA at any of the euthanasia time points. At 9–10 dpi and at 15–16 dpi, all live virus-inoculated pups that had bilirubinuria and acholic stools also had extrahepatic bile duct strictures and/or dilatations, while none of the saline inoculated or inactivated virus pups had bile duct strictures or dilatations (Fig. 2b). Two additional pups inoculated with live virus that had jaundice, oily hair, and stunted growth died at 15–16 dpi, before they could be assessed, and were excluded from the analysis.

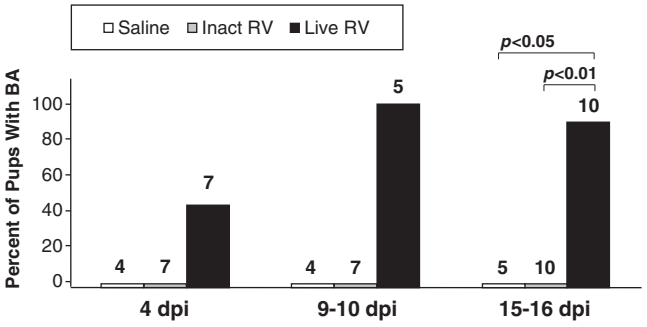

Fig. 1. Kinetics of development of BA in neonatal mouse pups. Mice were monitored for the development of BA (acholic stools, bilirubinuria, and, at 14–16 dpi, extrahepatic biliary strictures) at different times after inoculation with purified live triple-layered RRV particles (TLP), inactivated TLP, or saline. Total number of pups evaluated in each group is indicated above each bar. All mice that had acholic stools and bilirubinuria at 15–16 dpi had obvious extrahepatic bile duct and gallbladder abnormalities including strictures and dilatations, reflecting the specificity of objective assessment of stool and urine as a tool for detecting BA in this model.

Pups inoculated with live virus exhibited markedly stunted growth rates compared to inactivated virus or saline treated pups (Fig. 2c). The average weights of live virus-inoculated pups were significantly lower than the average weights of saline ($p<0.01$) and inactivated virus-inoculated pups ($p=0.01$) from 4 dpi to 15 dpi. Live RV treated pups began to lose weight daily beginning at 12 dpi. The weights of pups given inactivated virus were slightly but significantly lower than saline-inoculated pups 10 dpi through 16 dpi. Because pups inoculated with inactivated virus remained healthy and were visibly indistinguishable from saline-inoculated pups, their slightly lower weight is unlikely to be related to the experimental inoculation and unlikely to be biologically significant.

Sustained live RV antigenemia and transient inactivated RV antigenemia develop in neonatal mouse pups inoculated ip with RV

It has been recently discovered that RV circulates systemically in both animals and humans (Blutt et al., 2006, 2007). This finding has important implications for how RV might reach the biliary tract and for its role in pathogenesis of BA. There are no studies reporting antigenemia following inoculation of animals with inactivated RV, and no studies of the mouse BA model investigating antigenemia. To determine if intraperitoneal inoculation with inactivated RV can cause antigenemia in neonatal pups, pups were inoculated with live RV, inactivated RV, or with saline as described above, and serum was assessed for the presence of RV antigen at 1 day, 4 days, 9–10 days, or 15–16 days post-inoculation. RV antigen was undetectable in the serum of all saline-inoculated mice at all time points. RV antigen was detected in the serum of mice inoculated with live RV at all time points tested, based on ODs being above the lower limit of detection in this ELISA (0.094), and ODs were significantly higher than in saline-inoculated mice at all time points tested ($p<0.01$), although the mean OD at 15–16 dpi was low (Fig. 3). RV antigen was also detected in the serum of mice inoculated with inactivated virus at 1 dpi and not significantly different than in live RV treated mice at that time, although the mean OD was lower. Antigen levels in inactivated RV treated mice were significantly higher than in saline treated mice both at 1 dpi ($p<0.01$) and at 4 dpi ($p<0.05$). These findings demonstrate that serum RV antigenemia occurs in mice injected ip with the equivalent of 4×10^7 pfu inactivated RV up to 4 dpi.

In sum, intraperitoneal inoculation of newborn mice with a high dose of live RV caused sustained serum antigenemia (up to 15–16 dpi),

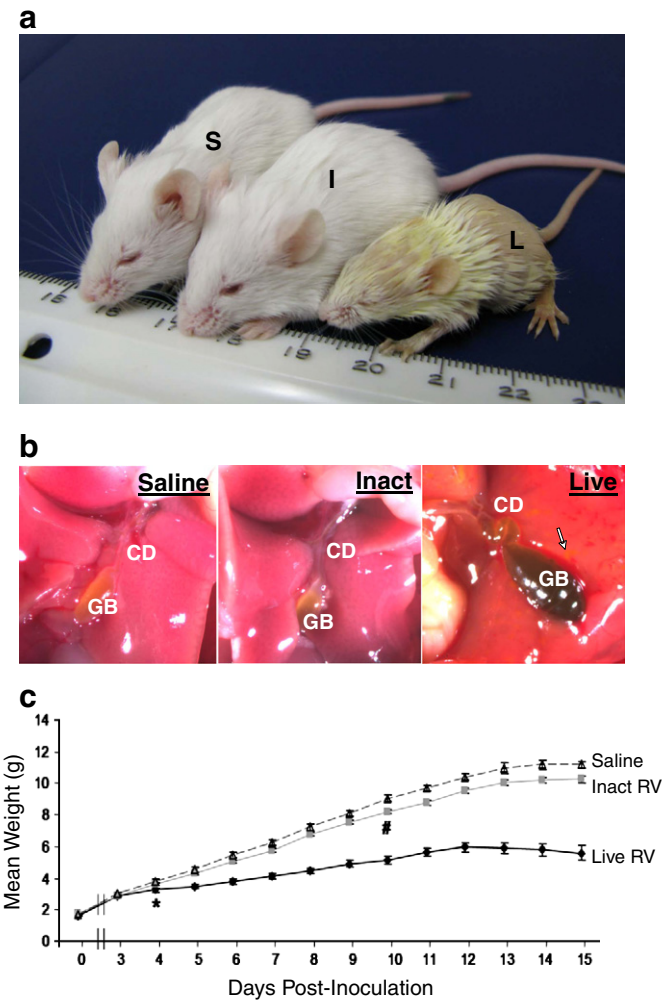

Fig. 2. RV-induced BA in a mouse model shares important clinical characteristics with human BA. (a) Jaundice and stunting of live RV-inoculated mouse with BA. Mouse inoculated with saline (S) weight 11.29 g; mouse inoculated with inactivated virus (I) weight 10.93 g; and mouse inoculated with live virus (L) weight 5.23 g at 16 dpi. Mice (S) and (I) had pigmented stools and normal urine, and mouse (L) had acholic stool, and bilirubinuria. (b) Liver and extrahepatic biliary tree of the same pups under dissecting microscope (~6×). Live RV-inoculated mouse liver has dark yellow hue, tortuous cystic duct (CD), necrotic foci (arrow) and distended, dark-colored gallbladder (GB) secondary to bile stasis. (c) Live RV-inoculated pups had significantly lower average body mass beginning at 4 dpi ($p<0.01$) compared with inactivated virus and saline treated pups (*). The average body mass of inactivated RV treated pups was slightly lower than that of saline treated pups, but this did not reach statistical significance until 10 dpi and after ($p=0.01$) (#).

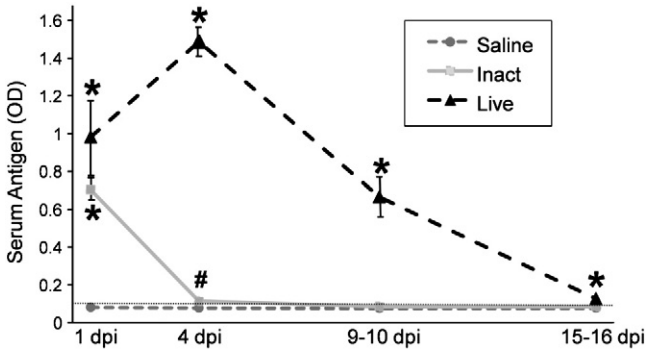

Fig. 3. Live and inactivated RV inoculated pups develop serum RV antigenemia. RV serum antigenemia at 1, 4, 9–10, and 15–16 dpi. For saline-inoculated pups, N = 16, 14, 4, 5, at 1 dpi, 4 dpi, 9–10 dpi, and 15–16 dpi, respectively. For inactivated RV-inoculated pups, N = 12, 7, 8, and 9 for the same time points. For live RV-inoculated pups, N = 4, 7, 7, and 7 for the same time points. The lower limit of antigen detection (0.094) is indicated with a thin horizontal line. (*) indicates $p<0.01$ vs saline treatment group. (#) indicates $p<0.05$ vs saline group. Inactivated RV vs live RV at 1 dpi was NS, and inactivated RV vs saline at 9–10 dpi and at 15–16 dpi was NS.

and intraperitoneal inoculation with the same dose of inactivated RV led to transient serum antigenemia. These results indicate that virus could be delivered to the biliary tree through the bloodstream.

Replicating RV and histopathology consistent with BA are observed in livers of mice injected with live but not inactivated RV

Infectious RV in liver extracts has been reported in the mouse model of BA, and RV capsid proteins have been identified in the bile duct epithelium of mice with RV-induced BA (Allen et al., 2007; Mohanty et al., 2010; Shivakumar et al., 2004). However, immune staining for nonstructural RV proteins, whose presence indicates replicating RV, has not been performed in the BA mouse model. To characterize histopathology in mice with BA and to determine if replicating RV is localized to infected biliary epithelium in the BA mouse model, we stained consecutive slides with hematoxylin and eosin and anti-RV or anti-NSP4. At 4 dpi, 38 of 59 (64%) portal tracts from five mice inoculated with live RV had portal expansion (inflammation), with inflammatory cells distributed in a concentric fashion around bile ducts (Fig. 4). In contrast, no inflamed or expanded portal tracts were observed in either inactivated RV-inoculated mice (90 portal tracts in 4 mice) or saline-inoculated mice (43 portal tracts in 3 mice).

In animals inoculated with live RV, but not in those inoculated with inactivated RV, viral capsid antigen-positive foci were present in 15 (25%) of 59 portal tracts assessed in 5 mice. In corresponding areas on consecutive sections, these RV-positive foci stained for cytokeratin 19 (CK-19), a bile duct epithelial cell marker, indicating that RV was present in bile ducts (Fig. 4). The RV nonstructural protein, NSP4, was also present in RV-positive foci on consecutive sections, indicating that viral replication was occurring in the infected cholangiocytes and that antigen had not simply been deposited in the bile ducts. There were no RV-positive portal tracts in inactivated RV-inoculated mice (90 portal tracts from 4 mice examined) or in saline inoculated mice (43 portal tracts from 3 mice examined) ($p<0.01$ live RV vs inactivated RV and live RV vs saline). Few RV-positive macrophages and hepatocytes and minimal lobular inflammation was observed in the live RV-inoculated pups at 4 dpi.

Fibrosis is an important feature in human BA, and has been described in the mouse BA model by approximately 2 weeks pi (Nadler et al., 2009). Picrosirius red staining, for fibrillar collagen, was performed on formalin-fixed sections from livers harvested at 15–16 dpi, and portal tracts were individually assessed for the presence of fibrosis (Fig. 5). Of 90 portal tracts assessed from the livers of five mice inoculated with live RV, 72 portal tracts (80%) had mild (nonbridging) fibrosis. There was no fibrosis, however, in the livers of mice inoculated with inactivated RV (115 portal tracts assessed in 4 mouse livers) or saline (96 portal tracts assessed in 3 mouse livers) ($p<0.01$ live RV vs inactivated RV and live RV vs saline).

Finally, bile ductular proliferation, a key histopathological feature of biliary atresia, was observed in the livers of all live RV-inoculated pups (with BA) at 15–16 dpi ($N=10$) but in none of the healthy pups treated with inactivated virus ($N=10$) or with saline ($N=5$). Proliferating bile ductules were readily apparent using immunohistochemistry with a CK-19 antibody (see below).

Osteopontin is expressed in all bile ducts in mice

Some studies have suggested that OPN may play a role in BA pathogenesis in humans (Bezerra et al., 2002; Huang et al., 2008;

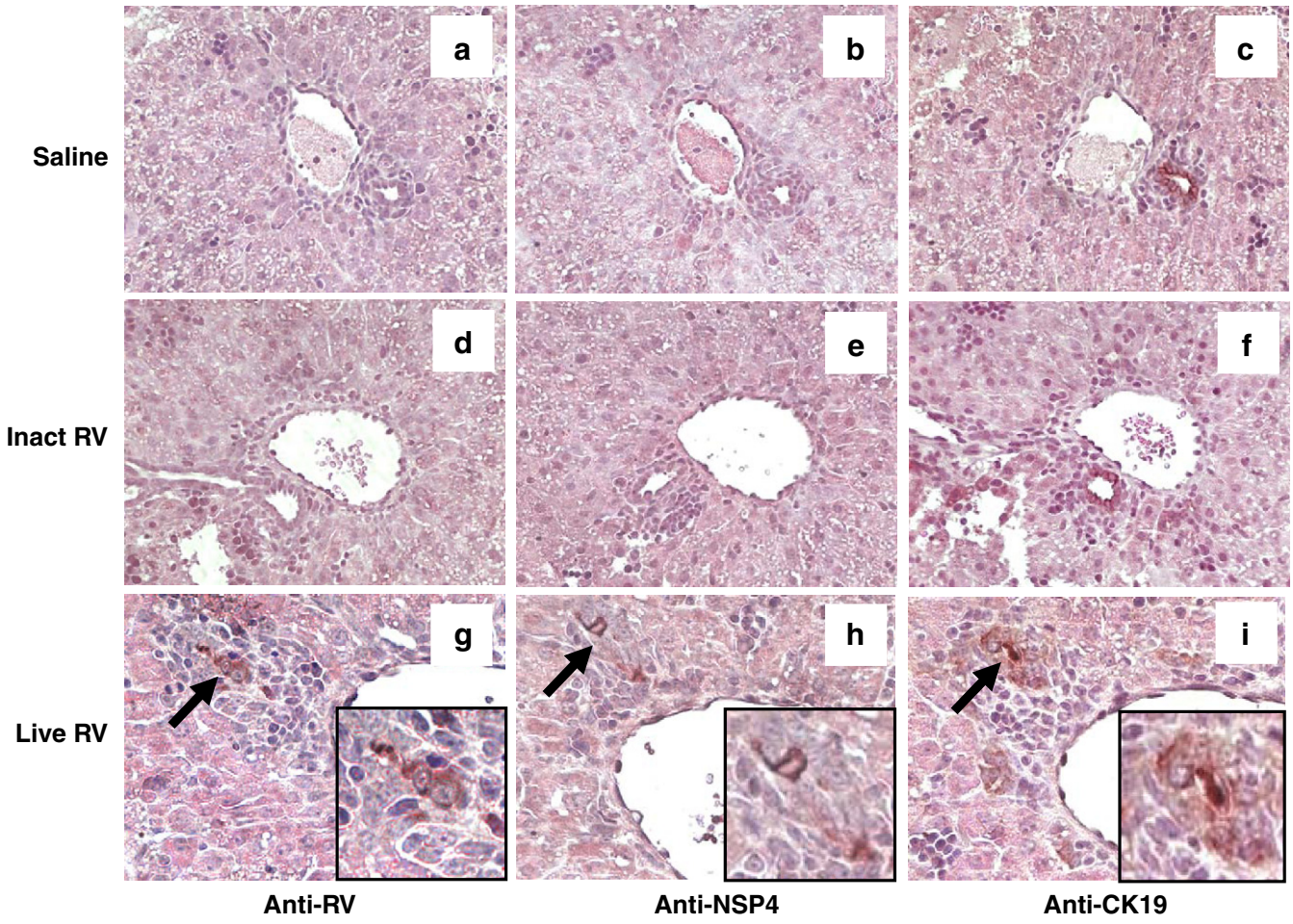

Fig. 4. Replicating virus is present in bile ducts of live RV-inoculated pups. Histopathology and RV, NSP4, and CK19 antigen detection in the livers of pups at 4 dpi. Bile ducts of saline (a–c) and inactivated RV (d–f) treated mice do not stain for RV or NSP4. Liver from RV-inoculated pup shows inflammation surrounding foci (arrows) that stain, on consecutive slides, for RV (g), the non-structural RV protein NSP4 (h), and cytokeratin 19 (bile ducts) (i), reflecting the presence of viral replication in bile ducts (20×). Insets show high-magnification images of virus-infected bile ducts, which are also highlighted using arrows (g–i).

Whitington et al., 2005). Patterns of OPN expression have been described in the livers and bile ducts of humans with BA in these studies but, to our knowledge, OPN expression in the livers of mice with RV-induced BA has not been described. Furthermore, previous studies characterizing OPN expression in human and mouse liver cite conflicting data with respect to expression in bile ducts in normal versus pathological states, and we sought to determine if OPN is expressed in all bile ducts or only in RV-infected or proliferating ducts in mice with BA (Brown et al., 1992; Huang et al., 2008; Whitington et al., 2005; Harada et al., 2003). To this end, we performed staining for osteopontin in formalin-fixed liver sections at early (4 dpi) and late (15–16 dpi) time points post-infection.

Using immunoperoxidase staining for osteopontin and CK-19 (bile duct epithelial marker) on consecutive formalin-fixed sections from livers harvested at 4 dpi, we observed osteopontin staining in areas corresponding to infected and uninfected bile ducts, although OPN staining was seen in slightly broader areas than CK-19 (Fig. 6a). To determine whether OPN and CK-19 truly colocalized, frozen sections

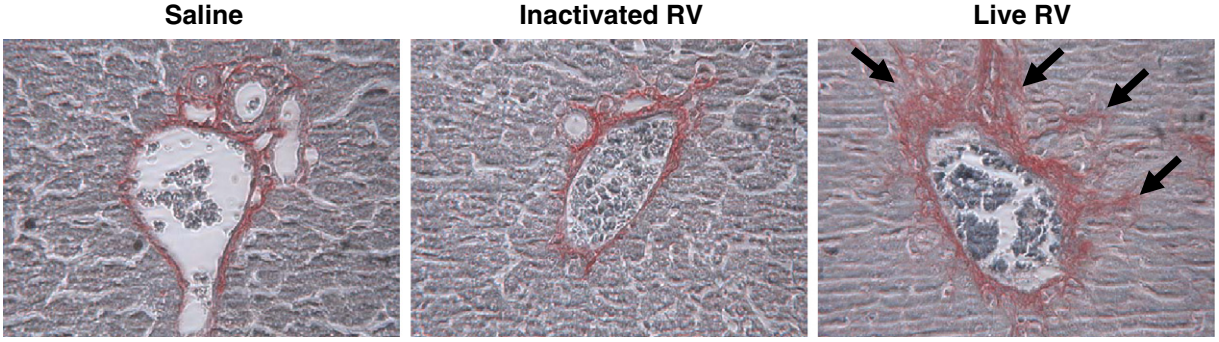

Fig. 5. Portal fibrosis is evident in mice inoculated with live RV (with BA) at 16 dpi. Healthy inactivated RV-treated mouse and saline control mouse livers have minimal staining limited to areas immediately adjacent to portal structures. The liver of a RV-injected mouse at 16 dpi (20×) stained with picrosirius red shows portal fibrosis (arrows).

of livers harvested at 14 dpi from a separate set of mice (inoculated with live RV) were costained for OPN and CK-19 using fluorescent secondary antibodies (Fig. 6b). Although the intensity of CK-19 staining in some cells was low, OPN and CK-19 did colocalize. This confirms that OPN was expressed in bile ducts in these specimens.

CK-19 and OPN staining on consecutive sections from 15 to 16 dpi livers of healthy mice (inoculated with inactivated RV or with saline) and mice with BA (inoculated with live RV) illustrated that OPN protein was expressed in proliferating and non-proliferating intrahepatic bile ducts and extrahepatic bile ducts of both sick and healthy mice (Figs. 7a–j). Cholangiocyte/bile duct proliferation occurs in response to biliary obstruction and is a cardinal histopathological feature of mouse and human BA (Petersen et al., 1997). We also observed OPN expression in the epithelium of extrahepatic bile ducts of mice with BA, including dense staining in an obstructed duct. The staining may represent inspissated bile (OPN is secreted in bile), but unlikely inflammatory cells, as the surrounding inflamed duct did not stain (Figs. 7i and j). To further confirm the specificity of the OPN staining, sections from the liver of a 6-week-old genetically osteopontin-deficient "knockout" mouse, on a BALB/c background, were analyzed. The bile ducts of a wild-type adult BALB/c control mouse stained positively (Figs. 7k and l), but no staining was seen in the bile ducts of the OPN-deficient mouse (Figs. 7m and n).

Osteopontin mRNA and protein expression is upregulated in livers of mice with BA

Bezerra et al. (2002) reported increased OPN mRNA in the livers of patients with BA compared with normal and non-BA disease controls. To determine if osteopontin expression is upregulated in the livers of mice with RV-induced BA, real-time RT-PCR was performed using RNA extracted from the livers of three groups of seven mice

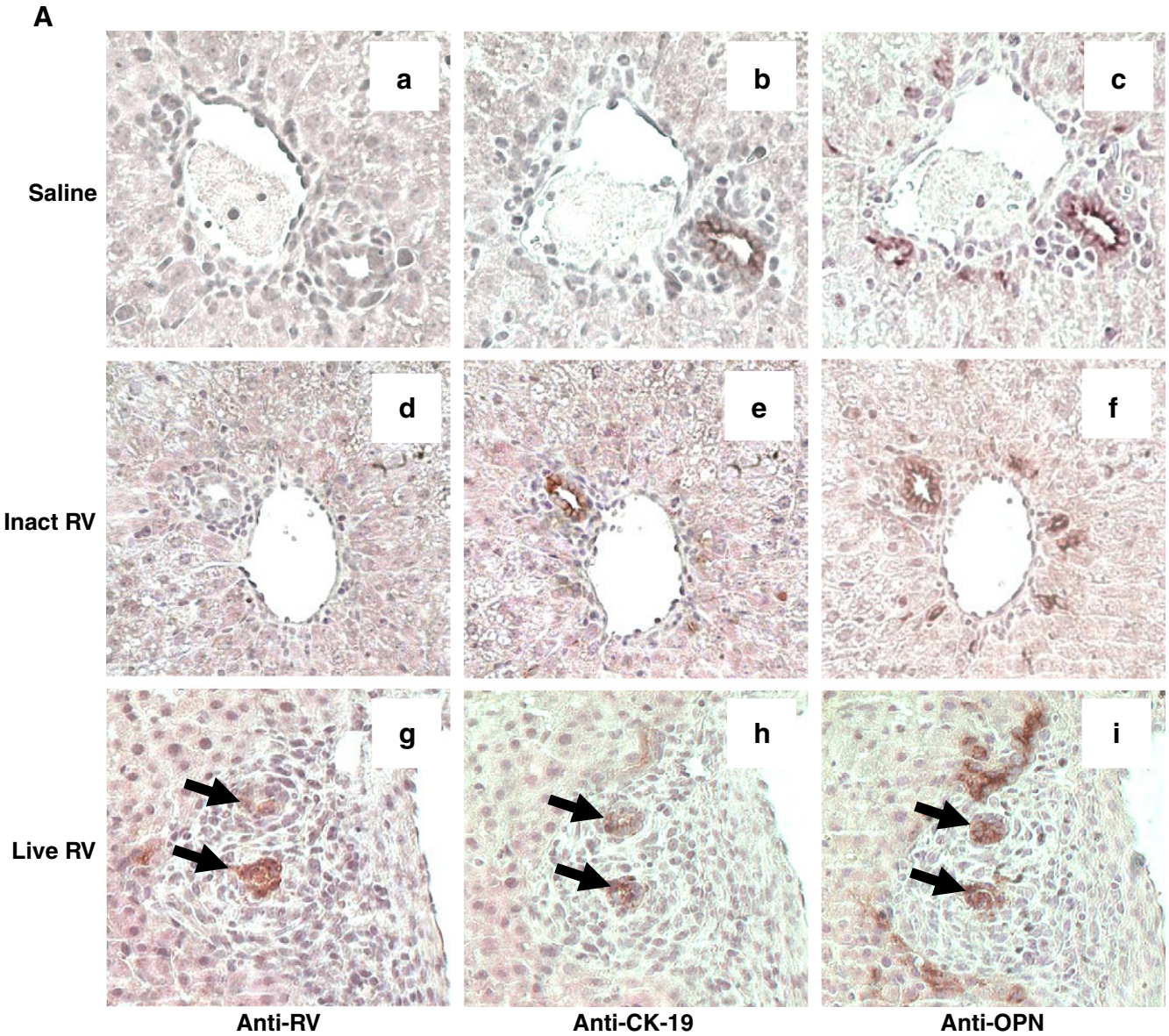

Fig. 6. Osteopontin (OPN) is expressed in RV-infected and in uninfected bile ducts. (A) Consecutive sections of formalin-fixed mouse liver 4 days post-inoculation with saline (a–c), inactivated RV (d–f), or live RV (g–i) (20×). Areas of RV, CK-19 (bile duct epithelium), and OPN staining are surrounded by dense inflammation in the liver of the live RV-inoculated mouse (g–i); arrows indicate RV-infected bile ducts. Normal bile ducts in saline- and inactivated virus-treated pups also stain for osteopontin in consecutive sections (a–f). (B) Merged immunofluorescent image (yellow) on frozen liver from a live RV-inoculated mouse with BA at 14 dpi (20×) shows similar staining patterns for CK19 (red) and OPN (green), although expression in some of the CK19-positive cells is relatively weak.

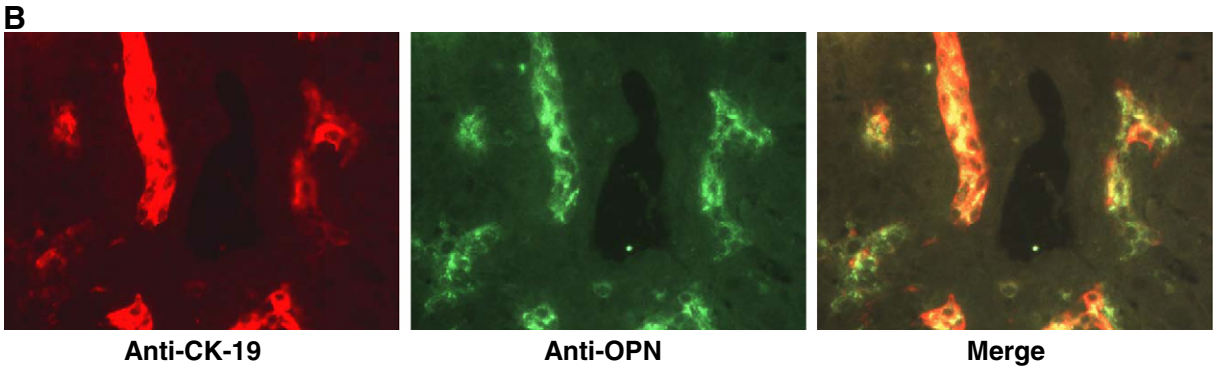

Fig. 6 (*continued*).

inoculated with 4×10^7 pfu live RV or inactivated RV, or saline. All live RV-injected mice developed BA, and none of the inactivated RV or saline inoculated mice developed BA. Osteopontin mRNA expression was upregulated 2.3-fold in live RV-infected mouse livers compared with the saline- or inactivated virus-inoculated mouse livers ($p<0.05$) (Fig. 8a). CK-19 was also assessed in order to determine if increased levels of OPN mRNA in the livers of mice with BA were secondary to increased numbers of cholangiocytes in association with cholangiocyte/bile duct proliferation, but CK-19 fold expression did not differ significantly between treatment groups. This indicates that cholangiocyte expression of OPN was upregulated in mice with BA, and that increased OPN mRNA in these livers could not be accounted for solely based on bile duct proliferation (and increased numbers of OPN-expressing cholangiocytes). To validate mRNA findings, OPN protein expression was assessed using Western blotting on protein extracted from the same snap-frozen livers used above. OPN protein expression was upregulated in livers of live RV-infected mice at 14 dpi compared with inactivated RV-treated or saline-treated mice at 14 dpi (Fig. 8b).

Rotavirus increases OPN expression in mouse cholangiocytes in vitro

RV infection of HT-29 intestinal epithelial cells causes upregulation of OPN expression and secretion *in vitro* (Rollo et al., 2005). To determine if RV increases OPN expression in cholangiocytes, immortalized BALB/c cholangiocytes were infected with RV, and OPN protein expression was assessed in cell lysates at 8, 24, or 48 h post-infection using Western blotting. OPN was slightly (i.e. 1.1 to 1.2 times) more abundant in RV-infected than in mock-infected cholangiocyte lysates, and densitometry analysis of immunoblots run using lysates from triplicate wells showed statistical significance at the 8 h time point (data not shown).

Osteopontin is not required for development of BA in rotavirus-infected neonatal mice

To determine if OPN is necessary for development of BA in the rotavirus mouse model, WT and genetically OPN-deficient (OPN−/−) 2-day-old Balb/c mouse pups were inoculated ip with 4×10^7 pfu RV (as above) or saline and assessed for BA, defined as acholic stools and bilirubinuria, beginning at 5–6 dpi.

The number of days of survival post-inoculation was also recorded up to 17 dpi. Days of survival pi for RV-injected WT mice were significantly more numerous than for RV-injected OPN−/− mice ($p<0.001$) (Fig. 9a).

All WT ($N=14$) and osteopontin-deficient ($N=10$) mice inoculated with RV developed bilirubinuria and/or acholic stools by 5–8 days pi (NS WT versus OPN-deficient RV-infected) (Fig. 9b). Injecting a lower dose of RV, 5.2×10^6 pfu, resulted in a slightly lower frequency of BA in both WT and OPN-deficient mice, but, again, there was no significant difference in OPN-deficient and WT rates of BA. None of the mice inoculated with saline ($N=10$ and $N=8$ for WT and osteopontin-deficient, respectively) developed bilirubinuria or acholic stools (saline-treated mouse BA data not shown).

WT and OPN-deficient mice treated with 5.2×10^6 pfu RV or saline were also assessed at 10 dpi for morphological abnormalities in the extrahepatic biliary tree under a dissecting microscope, and livers were then harvested for histopathological assessment. All WT RV-treated pups with acholic stools and bilirubinuria also had morphologic abnormalities of the extrahepatic biliary tree indicating extrahepatic biliary obstruction including distended gallbladders filled with darkly-colored bile and/or stones, and 3 of these pups also exhibited an irregular appearance to the common bile duct consistent with early development of strictures and/or dilatations. Among RV-treated osteopontin-deficient mice, 10 had an abnormal appearance to the gallbladder and three of these also had tortuous cystic ducts as seen in the WT mice with BA described earlier in this manuscript. Thus, at 10 dpi, there was evidence of cholestasis and extrahepatic biliary tree abnormalities in both WT and OPN-deficient RV-treated mice, and there were no distinguishable differences in rates of BA or extrahepatic biliary tree morphology between RV-infected WT and OPN-deficient mice.

Discussion

Our novel findings in the RV BA mouse model include demonstration that: (1) the dose of virus required to elicit BA is much greater than the dose required to infect neonatal pups; (2) transient RV antigenemia but not BA occurs following ip inoculation with inactivated RV. Also, protracted RV antigenemia, more persistent than previously reported in mice, occurs following inoculation with live RV; (3) RV replicates in cholangiocytes as evidenced by presence of the NSP4 in these cells; (4) hepatic osteopontin mRNA and protein expression is upregulated in mice with BA, which reflects findings in the livers of human BA patients, (5) OPN protein expression is modestly elevated in RV-infected cholangiocytes *in vitro*, and (6) osteopontin protein is expressed constitutively in all intrahepatic and extrahepatic bile ducts in normal (and diseased) mice.

Previous studies using the neonatal mouse model of BA inoculated mouse pups at 12–24 h of age with doses of RRV that ranged from 4×10^4 pfu to 1.5×10^6 ffu. Notably, these previous studies inoculated with a lower dose of virus and a younger age than we did and reported development of BA in ~60% to 80% of pups, respectively (Mack et al., 2005; Shivakumar et al., 2004). Higher rates of BA and mortality using an earlier inoculation age have clearly been demonstrated in this model previously (Czech-Schmidt et al., 2001). In our studies, we inoculated slightly older animals (24–48 h of age) to facilitate handling and determined that the dose of purified RRV administered by IP injection

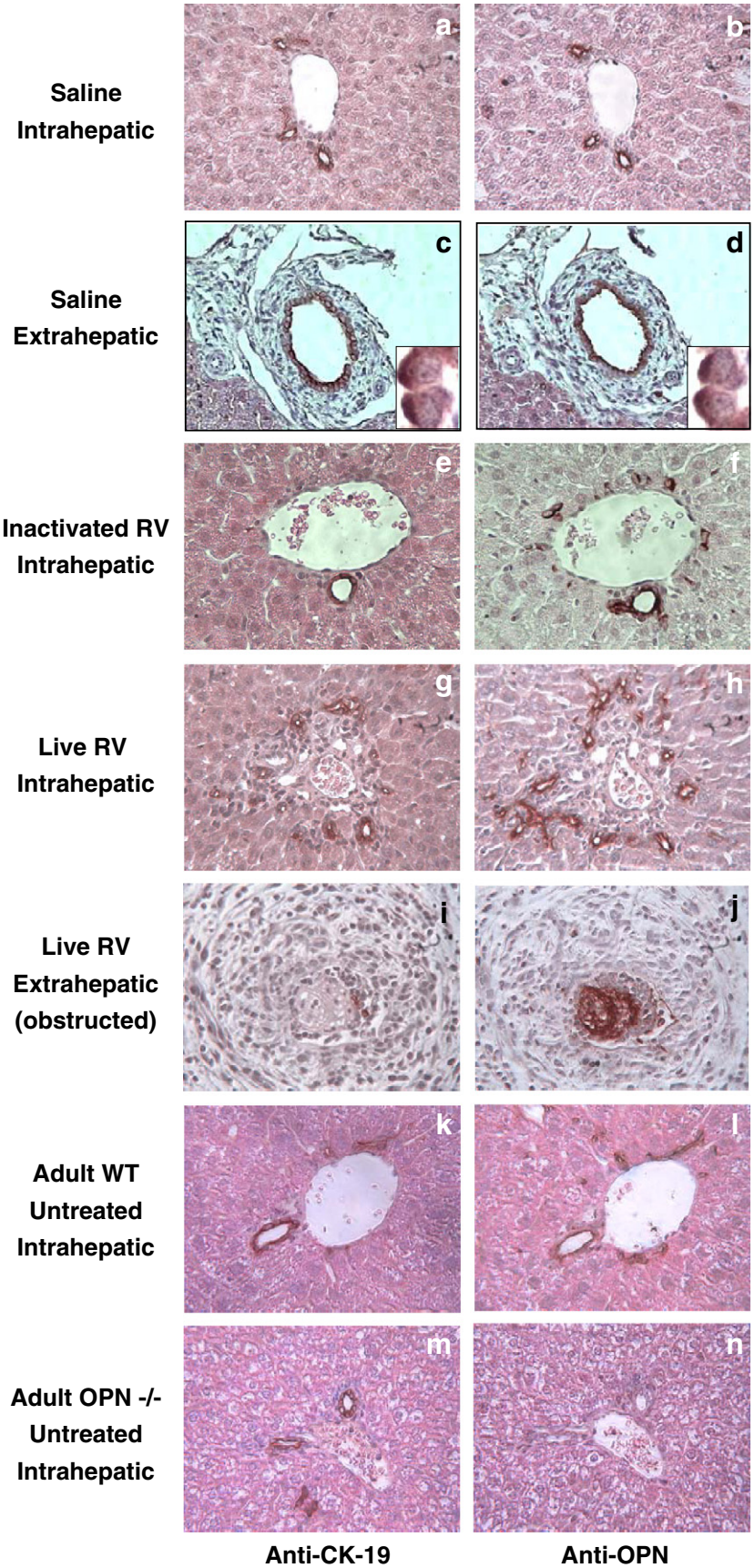

Fig. 7. Osteopontin is expressed in all intrahepatic and extrahepatic bile ducts. Consecutive sections of livers 15–16 days post-inoculation with saline (a–d), inactivated RV (e–f), and live RV (g–j), and in an untreated adult mouse (k–l). OPN is expressed in the cytoplasm and on the apical surface, an expression pattern that resembles that of CK-19 (insets c, d). There is no OPN staining of intrahepatic bile ducts in an OPN-deficient mouse (m–n).

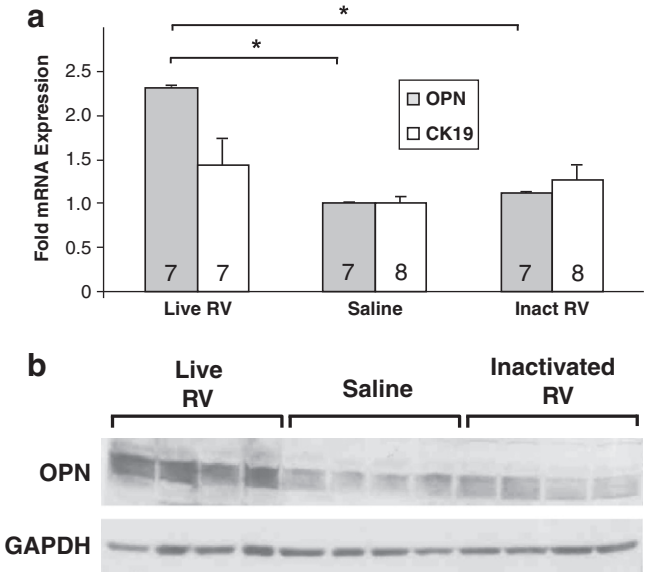

Fig. 8. Osteopontin expression is upregulated in livers of mice with BA. (a) OPN and CK-19 (bile duct epithelial cell/cholangiocyte marker) mRNA expression in livers of healthy inactivated virus- and saline-inoculated pups compared with livers from live RV-inoculated pups at 14 dpi, all of whom had BA (acholic stools and bilirubinuria) ($p<0.05$). Number of pups per treatment group indicated inside bars. (*) OPN expression in the livers of live RV-treated mice was significantly higher than in inactivated RV or saline treated mice ($p<0.05$). (b) OPN protein expression (60–65 kDa, with GAPDH loading control at 37 kDa) in livers of healthy inactivated virus- and saline-inoculated pups compared with livers from live RV-inoculated pups at 14 dpi with BA. Each lane represents the liver of an individual animal.

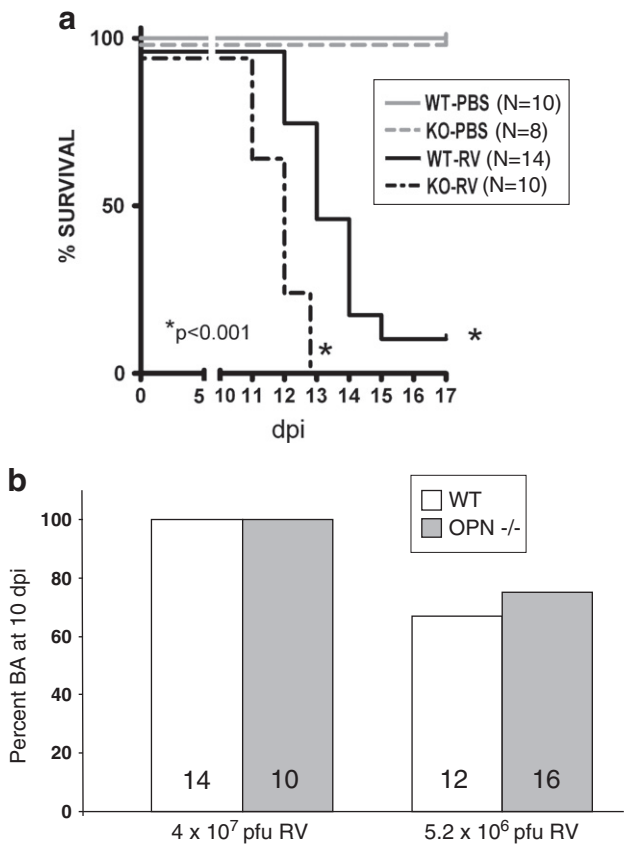

Fig. 9. OPN deficiency does not protect against RV-induced BA or improve survival. (a) Survival curve for WT and OPN-deficient mice inoculated with RV or saline ("PBS"). Survival was significantly longer in RV-inoculated WT mice (N = 14), of which two recovered, than in RV-inoculated OPN−/− mice (N = 10), of which none recovered ($p<0.001$). (b) Percent BA in WT and OPN−/− pups inoculated with two different doses of RV. N for each group indicated inside bars. Virus dose on X-axis. A slightly lower percentage of WT pups (67%) developed BA than OPN−/− pups (75%) at the lower RV dose, but this was NS.

needed to induce BA is significantly higher than the dose required to infect these mice based on induction of an antibody response.

No previous studies determined or compared the BA_{50} to the ID_{50} in this model, and the large difference in the BA_{50} compared to the ID_{50} (~10^4 fold higher) is remarkable. Although it remains unclear why such a high dose is needed, perhaps a large number of cholangiocytes in the liver need to be infected to trigger the cascade of immune-mediated events that cause BA in this mouse model while much smaller doses of virus can elicit a robust antibody response. This might indicate that cholangiocytes are somewhat resistant to infection but this restriction can be overcome by large doses of virus. Shivakumar et al. (2004) determined that the titer of RRV required to infect immortalized BALB/c mouse cholangiocytes in culture was 100 times higher than in MA104 cells (monkey kidney cell line, readily infected by rhesus RV). This relative resistance could also be a factor in the age-dependence of BA, with cholangiocytes from younger animals being more susceptible; this might explain why older mice do not get BA when given high doses of the same virus.

Our studies show that RV administered ip enters the circulation and virus antigen was detectable in serum at 25 hpi, the earliest time point examined. Antigenemia occurred whether the virus inoculated was live or inactivated. The initial systemic distribution of injected RV most likely occurred as a result of the virus passing directly into the vasculature from the peritoneum. The augmented and sustained antigenemia uniquely observed with live RV, however, was most likely supported by ongoing supply of new RV particles from infected epithelium (intestinal, biliary). Because natural RV infection begins in the intestine, it is possible that virus traveling through the bloodstream is an important mechanism by which RV is delivered to the biliary tree from the intestine. Lack of development of any feature of BA following injection with inactivated RV, despite transient antigenemia, indicates that replication of live RV in bile ducts is required to trigger the cascade of inflammatory events that leads to the bile duct destruction and progressive liver disease seen in this model. Although Shaw et al. (1995) reported that oral inoculation of 8- to 9-day-old mice with 1.5×10^6 ffu of inactivated RV caused mild diarrhea, we did not observe diarrhea or any other obvious sign of disease in neonatal mice inoculated ip with inactivated RV. Diarrhea is inconsistently seen in our neonatal mice inoculated with live RV, however, so lack of diarrhea with inactivated virus may not be surprising in this model.

While mice inoculated with inactivated RV did not develop biliary atresia, they had mild stunting of growth. There are several possible explanations for this observation. First, and most likely, there may have been an unequal sex distribution of pups between groups (males tend to weigh more than females as mice grow older); unfortunately, this was only considered after the data were analyzed, and sex was not able to be determined retrospectively. Secondly, the presence of serum antigenemia suggests that the inactivated virus particles circulated systemically and could theoretically have caused mild disease in any organ, affecting ponderal growth.

The feature of portal inflammation and fibrosis in our studies prompted us to examine expression of osteopontin in this BA mouse model because osteopontin plays roles in both inflammation and in fibrosis, and because it appears that it may contribute to BA pathogenesis in humans (Bezerra et al., 2002; Huang et al., 2008; Whitington et al., 2005). To our knowledge, hepatic osteopontin expression has not previously been studied in the BA mouse model. We have demonstrated that inoculation of neonatal mice with live RV leads to BA and upregulation of OPN expression concurrent with portal fibrosis, reflecting findings in livers of human BA patients (Bezerra et al., 2002; Huang et al., 2008; Whitington et al., 2005).

Osteopontin is a multifunctional glycoprotein that plays important roles in inflammation and fibrogenesis in numerous disease models (Cantor and Shinohara, 2009; Harada et al., 2003; Szalay et al., 2009; Vetrone et al., 2009) and could promote inflammation and/or fibrogenesis in BA. Our finding that osteopontin is expressed not only in proliferating bile ducts but also in normal intrahepatic bile ducts differs from findings in two studies of OPN expression in human BA in which, using different anti-OPN antibodies than the one we used, OPN was observed in proliferating bile ducts in non-syndromic BA but not in intrahepatic bile ducts of normal or disease controls (Huang et al., 2008; Whitington et al., 2005). One study, also using a different antibody than the antibody used in our experiments, described weak OPN protein expression in bile ducts of primary biliary cirrhosis patients but strong mRNA using in-situ hybridization (Harada et al., 2003). In an extensive survey of OPN expression in numerous human tissues, Brown et al. (1992) reported the presence of OPN mRNA in liver and gallbladder, localized to epithelia in both tissue types using immunohistochemistry and (in gallbladder epithelium) in-situ hybridization.

Other studies using mouse or human tissues have reported variable OPN staining patterns in the liver and bile ducts depending on which antibody was used (Fickert et al., 2007; Nakai et al., 2008). Different OPN antibodies may show apparently different expression patterns in the liver because OPN undergoes considerable post-translational modification, and antibodies made to OPN may bind to different OPN epitopes depending on the degree of post-translational modification of OPN when the antibody was made. Consistent with our findings, others have shown expression of osteopontin in normal intrahepatic mouse bile ducts using the antibody we used (Fickert et al., 2007), and lack of bile duct staining in a genetically osteopontin-deficient mouse in our studies confirms specificity of this antibody. We also observed OPN staining of occasional inflammatory cells identified morphologically in RV-treated mice, but have not characterized this finding further. OPN is known to be expressed by several types of inflammatory cells (Whitington et al., 2005).

We were able to demonstrate a modest upregulation of OPN expression in RV-infected cholangiocytes *in vitro* under the conditions we tested, and the vast majority of OPN-expressing cells in the liver are cholangiocytes. It is likely that upregulated expression in cholangiocytes accounts for the increased hepatic OPN we observed in mice with BA, but perhaps OPN expression is more highly upregulated in cholangiocytes *in vivo* than *in vitro* because indirect effects of RV infection are operative in the liver, such as a cytokine or chemokine-mediated effects. IFN-γ is a highly upregulated cytokine in the livers of mice with BA and an important mediator of bile duct obstruction in this model (Shivakumar et al., 2004). Barnes et al. (2008) observed that incubation of immortalized BALB/c cholangiocytes with IFN-γ induced expression of a broader spectrum of cytokines and chemokines, including IL-6 and TGF-β, than incubation with RV. IFN-γ induces OPN expression in monocytoid cells (X. Li et al., 2003; Z. Li et al., 2003). It is thus possible that IFN-γ stimulates cholangiocytes to increase OPN expression *in vivo*. This is a question that merits further investigation.

In considering the data we present here along with previously reported findings, OPN is apparently upregulated only in intrahepatic, but not extrahepatic, biliary epithelium in the RV mouse model of BA (human extrahepatic bile ducts have not been studied) (Carvalho et al., 2005). It is thus possible that OPN is specifically upregulated in proliferating bile ducts, which are located only within the liver. Several types of proliferating cells may have increased expression of OPN (De Barros et al., 2010; Sun et al., 2009; Whitington et al., 2005). Alternatively, upregulation of OPN in intrahepatic and not extrahepatic cholangiocytes could potentially result from any of a multitude of liver-specific factors that extrahepatic bile ducts are not exposed to. The milieu of the liver differs significantly from that of the extrahepatic biliary tree, with the presence of hepatocytes, resident Kupffer cells, and other cell types that contribute to the immune response (Racanelli and Rehermann, 2006). Furthermore, cholangiocytes of the intrahepatic bile ducts differ morphologically and functionally from cholangiocytes of the extrahepatic bile ducts, and have different transcriptional profiles (Glaser et al., 2010). Each of these differential features of the liver and extrahepatic bile ducts could help to explain differences in intrahepatic versus extrahepatic biliary OPN expression in BA, and should be examined in future studies focusing on BA pathogenesis.

Because OPN has Th1 cytokine activity and a Th1 response to RV infection of cholangiocytes leads to BA in the mouse model, we were surprised to discover that it is not critical for disease (Mack et al., 2005; Shivakumar et al., 2004). Because inflammation involves redundant pathways, a compensatory response to RV infection and bile duct obstruction in OPN-deficient mice may be occurring. OPN may thus be contributory in disease pathogenesis in this model, but we have shown that it is not critical. In a DDC-induced mouse model of primary sclerosing cholangitis, an obstructive cholangiopathy (like BA is), it was found that OPN-deficient mice had similar degrees of disease severity as WT mice in several aspects, including degree of inflammation and fibrosis, indicating that OPN is not critical for disease in this model, either (Fickert et al., 2010). OPN is also not critical for disease in carbon tetrachloride-induced hepatocellular toxicity and, in fact, OPN-deficient mice have more severe necrosis and fibrosis than WT mice in this model (Lorena et al., 2006). In a nonalcoholic steatohepatitis (NASH) mouse model, however, OPN appears to play a protective role (Sahai et al., 2004). OPN-deficient mice had less severe inflammation and fibrosis despite similar degrees of steatosis in this study. Interestingly, an anti-TNF agent also reduced inflammation in this model, in which TNF-α expression is upregulated, whereas anti-TNF treatment had no beneficial effect on disease in the BA mouse model, in which TNF-α is also upregulated (X. Li et al., 2003; Z. Li et al., 2003; Mack et al., 2005). Further dissection of the immune responses in each of these disease models is required to elucidate pathways that are distinct in each and to provide some explanation for why inhibition of OPN and of TNF-α have distinct effects.

Conclusions

In conclusion, we report novel findings in an established mouse model of RV-induced BA that shed new light on viral pathogenesis and on the potential role of OPN, a molecule with pro-inflammatory and pro-fibrogenic activity that potentially plays a role in pathogenesis of human BA. For the first time, we report that inactivated RV serum antigenemia, which, despite implications for delivery of inactivated RV to the liver, does not lead to BA. We have shown that high doses of replicating RV, well above doses required to elicit a humoral immune response, are required to elicit BA in this model, and that NSP4 is expressed in cholangiocytes of animals with BA, providing evidence of RV replication in these cells. We have shown that OPN is constitutively expressed in the intra- and extra-hepatic bile ducts of normal mice as well as in the bile ducts of mice with BA, a finding that has not been consistently reported in the literature or widely acknowledged. We also report increased OPN expression in the livers of mice with BA, as has been previously reported in the livers of human BA patients, which is most likely secondary to increased production on OPN by cholangiocytes in affected mice. Although we observed only slightly increased OPN upregulation in RV-infected cultured cholangiocytes, it is likely that additional factors present in the livers of diseased mice indirectly cause increased OPN production. Finally, we show, for the first time, that OPN is not necessary for development of BA in the RV mouse model and, in fact, hastens mortality. The shortened life span we observed in OPN-deficient RV-infected mice may be related to direct effects of RV pathogenesis, as opposed to immune-mediated liver damage, since OPN functions as a cytokine and appears to be protective in a RV diarrhea model (Rollo et al., 2005). This needs to be examined further. Because inflammation appears to be critical for disease in this model (Shivakumar et al., 2004), and because fibrosis also occurs and is severe in humans with BA,

mechanisms of inflammation and fibrogenesis that are independent of OPN need to be examined. Further studies in the BA mouse model as well as in DDC cholangitis and NASH mouse models could provide valuable insight.

Materials and methods

Viruses

The simian rhesus RV (RRV) (P5[3], G3, isolated from the feces of a 3.5-month-old rhesus monkey with diarrhea) was kindly supplied by H. B. Greenberg (Stanford University Medical School, Palo Alto, CA) and was cultivated in African green monkey kidney cells (MA104) in the presence of trypsin as described previously (Crawford et al., 2001). Triple layered RRV particles were purified using CsCl density gradient centrifugation, and titration of purified virus was determined by plaque assay (Estes et al., 1979). An aliquot of purified virus was then used to prepare psoralen-inactivated virus (PI-RRV) by incubation with 4′-aminomethyl-4,5′,8-trimethyl psoralen (40 μg/ml for 40 min on ice under A_{365} UV light) (Groene and Shaw, 1992). Inactivation of virus was confirmed by 3 sequential passages in MA104 cells for 24 h each. Media collected from each passage were tested for infectious virus by plaque assay, and no plaques were detected from any of the samples. A separate aliquot of PI-RRV was prepared for use in a separate experiment whereby frozen livers were obtained at 14 dpi to assess OPN expression. Performance of a plaque assay determined that the titer of live virus in this aliquot of PI-RRV was $<5\times10^4$ pfu/ml. The concentrations of both aliquots of antigenically intact psoralen-inactivated virus particles were determined to be comparable to the stock of live virus from which they were taken using a hemagglutination assay as described previously (Kalica et al., 1978).

Animal inoculations

Newborn BALB/c WT or OPN-deficient mouse pups (the latter kindly donated by Dr. Harvey Cantor, Harvard University) were inoculated intraperitoneally (ip) at 24 to 48 h of life with 4×10^7 pfu live RRV triple-layered particles suspended in 40 μl Tris sodium chloride-10 mM $CaCl_2$ (TNC; hereafter "saline"); with an equivalent amount of antigenically intact (confirmed by hemagglutination assay), psoralen/UV inactivated RRV triple-layered particles suspended in saline; or with saline lacking virus (control animals). RV dose was 4×10^7 pfu in all experiments with the exception of the experiment where OPN-deficient and WT mice were assessed and euthanized at 10 dpi; RV dose in this case was 5.2×10^6 pfu. All inoculations were 40 μl in volume, administered using a 1 cm^3 syringe with a 33G, 1/2 cm needle using a repeating dispenser (Hamilton Company, Reno, NV).

Assessment for biliary atresia

Beginning at 4–5 days post inoculation (dpi), all mouse pups were assessed daily for signs of cholestasis in the following order: animals inoculated with PBS, animals inoculated with inactivated virus and, lastly, animals inoculated with live virus. The weight in grams, to two decimal points, of all pups in each litter (allowing for calculation of mean pup weight for each litter) was recorded on the day of inoculation and, beginning at 3 dpi, the weight of each individual pup was recorded daily until the pup died or was euthanized. Stool and urine were elicited when possible by gently palpating the abdomen. Stool color was assessed by colorimetric scale using a paint color swatch RC11 (Glidden/ICI Paints, Cleveland, OH). Acholic stool was defined as stool color 1 (Wood Lily, 40YY 83/129), stool color 2 (Corn Silk, 40YY 77/242), or stool color 3 (Sweet Corn, 30YY 58/423). Stool color 4 (Golden Marguerites, 20YY 37/654) was defined as not acholic (i.e. normal). Urine was assessed for direct bilirubin content using the bilirubin index on a rapid Multistix dipstick test per package instructions (Bayer Corporation, Elkhart, IN). Bilirubinuria was defined as high (+++) urine bilirubin content. Biliary atresia was defined as presence of acholic stool and bilirubinuria at time of euthanasia and, in mice euthanized at the 14–16 dpi time point, visible extrahepatic biliary tree strictures, dilatations, and/or cystic duct tortuosity as viewed under the dissecting microscope ~6× (described below). All 9 mice examined at 14–16 dpi that had bilirubinuria and acholic stools had obvious extrahepatic biliary dysmorphology, reflecting the specificity of objective stool and urine assessment alone to define BA in this model.

Serum and tissue sample collection and processing

At 4, 9–10, or 15–16 days post-inoculation (dpi), each pup was anesthetized with isoflurane and decapitated. Blood from the neck vessels was placed in a plasma separator tube (Becton Dickinson and Company, Franklin Lakes, NJ). The tube was centrifuged at 10,000 rpm for 5 min, and the serum was stored in a separate microcentrifuge tube at 4 °C pending analysis. The abdomen and chest were opened with a single longitudinal incision, and the extrahepatic bile ducts, gallbladder, and liver were examined under a dissecting microscope (6×). Extrahepatic bile duct and cystic duct gross morphology was described by noting the presence or absence of marked tortuosity, strictures, and/or cystic dilatations. The liver and extrahepatic bile ducts were then removed by first resecting the anterior lobes and then the remainder of the liver, extrahepatic bile ducts and a small portion of duodenum was removed en block (4 dpi or 9–10 dpi), or in a similar fashion without first resecting the anterior lobes (15–16 dpi). Tissues were allowed to fix in 10% neutral-buffered formalin overnight and then stored in 70% ethanol for dehydration until paraffin embedding and sectioning was performed (below). In some experiments designed to allow performance of fluorescent immunohistochemistry and qRT-PCR on frozen livers, livers were harvested and snap frozen using liquid nitrogen.

Evaluation of histology and immunohistochemistry

To evaluate histopathology, formalin-fixed, paraffin-embedded sections were stained with TROMA III rat anti-cytokeratin 19 (CK19) (Developmental Studies Hybridoma Bank, Iowa City, IA), rabbit anti-RV serum made against lapine RV strain ALA (Blutt et al., 2007), rabbit anti-NSP4 peptide 114–135, or goat anti-mouse osteopontin (R & D Systems, Minneapolis, MN). The Vectastain Elite ABC kit (Vector Laboratories, Burlingame, CA) and liquid 3,3′-diaminobenzidine (BioGenex, San Ramon, CA) were used as recommended by the manufacturer. Staining for CK19, RV, and osteopontin was performed on consecutive sections from each mouse liver. NSP4 (nonstructural RV protein) and picrosirius red (fibrillar collagen staining for fibrosis; Polysciences, Inc., Warrington, PA) staining was performed on nonconsecutive and on a few consecutive sections. Immunofluorescent co-staining was performed on snap-frozen liver sections harvested at 14 dpi (see above) using TROMA III anti-CK19 and anti-osteopontin primary antibodies followed by secondary Alexa-Fluor (Invitrogen, Carlsbad, CA).

Determination of ID_{50} and BA_{50}

BALB/c mouse pups at 24–48 h of age were inoculated intraperitoneally with 40 μl of 10-fold serial dilutions of rhesus RV live purified triple layered particles. Each dose was given to 4–10 pups. At 14 dpi, pups were evaluated for BA, as described above, then euthanized and serum collected to detect RV-specific antibody by ELISA. The ID_{50}, defined as the dose required to induce detectable (i.e. a titer of 50 or higher) anti-RV serum antibody in 50% of pups, and the BA_{50}, defined as the dose required to induce acholic stool, bilirubinuria, and visible strictures or dilatations (at 6×) of extrahepatic bile ducts in 50% of mice were calculated by the method of Reed and Muench, as described previously (Reed and Muench, 1938).

Detection of serum total RV antibody by ELISA

ELISA was performed in 96-well polyvinyl chloride microtiter plates (Dynatech, McLean, VA). The plates were coated with guinea pig serum (diluted 1:5000 in carbonate bicarbonate buffer pH 9.6) containing anti-SA11 RV antibody, blocked with blotto (5% [wt/vol] Carnation powdered milk in PBS) and washed. SA11 RV was added in a concentration necessary to obtain a standard titer of the positive control rabbit serum and 1/10 blotto was added as a negative antigen control for each well. The plates were incubated at 37 °C for 1 h and washed, then test samples were added serially diluted twofold down the plate and incubated again for an hour. After another wash, horseradish peroxidase-conjugated goat anti-rabbit IgA, IgM, and IgG (Kirkegaard and Perry Laboratories, Gaithersburg, MD) were added at a concentration of 1:10,000 with 5% normal guinea pig serum, incubated for an hour, and plates were washed. TMB Micro-well ELISA substrate (Kirkegaard and Perry Laboratories, Gaithersburg, MD) was added and allowed to react for 10 min at room temperature, and the reaction was stopped by the addition of an equivalent volume of 1 M H_3PO_4. Optical densities (ODs) at 450 nm were determined with a SpectraMax M5 microplate reader (Molecular Devices, Sunnyvale, CA). A sample was considered positive if the OD450 value of the virus well minus the control well was greater than 0.1. Additionally, an endpoint titer of the positive control serum (run on each plate) had to be within two dilutions of an established standard for the test to be acceptable. Antibody titer for each sample was defined as the inverse of the lowest dilution that tested positively, and detectable antibody was considered present in samples with titers of 50 or greater.

Detection of RV antigen by ELISA

Serum samples were evaluated for the presence of RV antigen by ELISA. ELISAs were performed in 96-well polyvinyl chloride microtiter plates (Dynatech, McLean, VA). The plates were coated with mouse ascites (diluted 1:20,000 in carbonate bicarbonate buffer pH 9.6) containing anti-VP6 6E7 monoclonal antibody in carbonate–bicarbonate buffer (pH 9.6) and incubated overnight at room temperature. The plates were blocked with 200 μl of 5% blotto (5% [wt/vol] Carnation powdered milk in PBS) for 2 h at 37 °C. Following removal of the blotto, the plates were washed three times with 0.05% Tween 20 in PBS. The serum samples, in 20 μl aliquots, were treated with 50 mM EDTA. Hyperimmune guinea pig serum to SA11 RV diluted (1:2000) in 1/10 blotto was used as the detector antibody. Horseradish peroxidase-conjugated goat anti-guinea pig immunoglobulin G (Sigma) diluted (1:1000) in 1/10 blotto with 2.5% fetal calf serum was used as the conjugate. TMB Micro-well ELISA substrate (Kirkegaard and Perry Laboratories, Gaithersburg, MD) was added and allowed to react for 10 min at room temperature, and the reaction was stopped by the addition of an equivalent volume of 1 M H_3PO_4. Optical densities (ODs) at 450 nm were determined with a SpectraMax M5 microplate reader (Molecular Devices, Sunnyvale, CA). A cutoff value for detectable antigen was defined as greater than or equal to the mean of the ODs of the PBS control animal samples plus 3 standard deviations.

RV infection of immortalized cholangiocytes

Media containing RRV (at an MOI of 50, which is the equivalent of 50 virus particles per cell, as used previously in this cell line) (Barnes et al., 2008; Jafri et al., 2009), or virus-free media were incubated for 1 h with confluent murine cholangiocytes, a cell line derived from WT Balb/c mice (Mano et al., 1998). Thereafter, cells were incubated with virus-free medium for predetermined time intervals. Media were then aspirated and cells were treated with ice cold PBS and lysed for total protein extraction using 50 mM Tris buffer, pH 7.5, containing 2 mM EDTA and EGTA, 0.5 M NaCl, 1% Triton-X 100, 0.25% DOC, and protease inhibitors. The experiment was performed in triplicate and blots were analyzed using densitometry.

Immunoblot analysis

Cell lysates from RV-infected or mock-infected BALB/c cholangiocytes were mixed with SDS-PAGE sample buffer, boiled for 5 min, and loaded onto 12 or 12.5% polyacrylamide gels (BioRad). Protein from cell culture media was concentrated using Vivaspin 10,000 MWCO columns (Sartorius Stedim Biotech, Goettingen, Germany) prior to loading onto polyacrylamide gels. Flash-frozen mouse liver (14 dpi) was homogenized in lysis buffer and quantity of total protein was determined using the BCA protein assay method (Pierce, Rockford, IL) before loading 100 μg of each sample onto a polyacrylamide gel as above. After each gel electrophoresis was complete, protein samples were transferred onto nitrocellulose membranes (GE Healthcare Bio-Sciences Corp., Piscataway, NJ) as previously described (Zhang et al., 2000). Membranes were blocked using 5% Carnation Instant Milk in PBS (Blotto) for 10 min with agitation at room temperature. Proteins were detected with antibodies against recombinant mouse osteopontin (R&D Systems, Minneapolis, MN) at a dilution of 1:10,000 1:250, rat cytokeratin 19 (Developmental Studies Hybridoma Bank, Iowa City, IA) at a dilution of 1:250, or GAPDH (Abcam, Philadelphia, PA) at a dilution of 1:5000 in 0.5% blotto. Alkaline phosphatase or horseradish peroxidase-conjugated secondary antibodies (Sigma-Aldrich, St. Louis, MO) were used at a dilution of 1:3000 in 0.5% blotto. Membranes were incubated with the primary antibodies at room temperature overnight, washed 3 times for 5 min in 0.5% blotto, and incubated with the secondary antibodies for approximately 2 h. The membranes were again washed 3 times for 5 min in 0.5% blotto and were developed using alkaline phosphatase detection solution (50 mM Tris, 3 mM $MgCl_2$, 0.1 mg/ml p-nitro blue tetrazolium chloride, and 0.05 mg/ml 5-bromo-4-chloro-3-indolyl phosphate).

Quantitation of osteopontin and CK-19 mRNA

Levels of osteopontin mRNA expression in RV or saline inoculated animals were determined in livers harvested and snap frozen at 14 dpi. RNA was extracted from a portion of each liver using RNEasy kit (Qiagen, Valencia, CA) according to the manufacturer's instructions, and extracts were treated with DNAse. cDNA was synthesized using the High Capacity cDNA Reverse Transcription Kit (Applied Biosystems, Carlsbad, CA) according to the manufacturer's instructions. Real-time RT-PCR was then performed using SYBR green Master Mix (Applied Biosystems, Carlsbad, CA) with 2 μg cDNA and 100 μM each primer (OPN Fwd: 5′-ACA CTT TCA CTC CAA TCG TCC-3′; Rev: 5′-TGC CCT TTC CGT TGT TGT CC-3′, CK19 Fwd: 5′-CTCGGATTGAGGAGCTGAAC-3′; Rev: 5′-TCACGCTCTGGATCTGTGAC-3′). The RNA isolation protocol included DNAse treatment to remove contamination of genomic DNA. Moreover, RT-PCR sense and antisense primers were designed so that target sequences span across intron–exon junctions ensuring amplification of mRNA and not DNA. Results were normalized to β-actin (primers: Fwd 5′-CCT TGC AGC TCC TTC GTT GC-3′; Rev 5′-ACG ATG GAG GGG AAT ACA GC-3′).

Statistical analysis

Student's t-test was used to compare serum antigen levels, daily weights, and osteopontin and CK-19 mRNA expression. Statistically significant differences between treatment groups in terms of frequency of biliary atresia, RV in portal tracts, portal inflammation, and portal fibrosis were determined using a z-test for comparison of two proportions. Kaplan–Meier survival analysis was performed using Graphpad Prism software (San Diego, CA).

Acknowledgments

The research contained in this report was supported in part by Public Health Service grants R01 AI080656 (to M.K.E.), P30 DK56338 that funds the Texas Medical Center Digestive Diseases Center, and by an American Gastroenterological Association/Astra Zeneca

Fellowship/Faculty Transition Award, NIHK12 HD41648, and NASPGHAN/CDHNF Young Investigator Development Award (to P.M.H.).

We thank Harvey Cantor, M.D. (Harvard Medical School) for providing breeding pairs of osteopontin-deficient mice, Brooke Bessard and Bryan Tackett (Baylor College of Medicine) for their technical assistance, and Sarah Blutt, Margaret Conner, Joseph Hyser, and Sundararajah Thevananther (Baylor College of Medicine) for their helpful feedback.

References

Allen, S.R., Jafri, M., Donnelly, B., McNeal, M., Witte, D., Bezerra, J., Ward, R., Tiao, G.M., 2007. Effect of rotavirus strain on the murine model of biliary atresia. J. Virol. 81 (4), 1671–1679.

Barnes, B.H., Tucker, R.M., Wehrmann, F., Mack, D.G., Ueno, Y., Mack, C.L., 2008. Cholangiocytes as immune modulators in rotavirus-induced murine biliary atresia. Liver Int. 29 (8), 1253–1261.

Bezerra, J.A., Tiao, G., Ryckman, F.C., Alonson, M., Sabla, G.E., Shneider, B., Sokol, R.J., Aronow, B.J., 2002. Genetic induction of proinflammatory immunity in children with biliary atresia. Lancet 360, 1653–1659.

Blutt, S.E., Fenaux, M., Warfield, K.I., Greenberg, H.B., Conner, M.E., 2006. Active viremia in rotavirus-infected mice. J. Virol. 80 (13), 6702–6705.

Blutt, S.E., Matson, D.O., Crawford, S.E., Staat, M.A., Azimi, P., Bennett, B.L., Piedra, P.A., Conner, M.E., 2007. Rotavirus antigenemia in children is associated with viremia. PLoS Med. 4 (4), e121.

Brown, L.F., Berse, B., VanDeWater, L., Papadopoulos-Sergiou, A., Perruzzi, C.A., Manseau, E.J., Dvorak, H.F., Senger, D.R., 1992. Expression and distribution of osteopontin in human tissues: widespread association with luminal epithelial surfaces. Mol. Biol. Cell 3, 1169–1180.

Cantor, H., Shinohara, M., 2009. Regulation of T-helper-cell lineage development by osteopontin: the inside story. Nat. Rev. Immunol. 9 (2), 137–141.

Carvalho, E., Liu, C., Shivakumar, P., Sabla, G., Aronow, B., Bezerra, J.A., 2005. Analysis of the biliary transcriptome in experimental biliary atresia. Gastroenterology 129 (2), 713–717.

Crawford, S.E., Mukherjee, A.K., Estes, M.K., Lawton, J.A., Shaw, A.L., Ramig, R.F., Prasad, R.V., 2001. Trypsin cleavage stabilizes the rotavirus VP4 spike. J. Virol. 75, 6052–6061.

Czech-Schmidt, G., Verhagen, W., Szavay, P., Leonhardt, J., Petersen, C., 2001. Immunological gap in the infectious animal model for biliary atresia. J. Surg. Res. 101, 62–67.

De Barros, A.P., Takiya, C.M., Garzoni, L.R., Leal-Ferreira, M.L., Dutra, H.S., Chiarini, L.B., Meirelles, M.N., Borojevic, R., Rossi, M.I., 2010. Osteoblasts and bone marrow mesenchymal stromal cells control hematopoietic stem cell migration and proliferation in 3D in vitro model. PLoS One 5 (2), e9093.

Domiati-Saad, R., Dawson, D.B., Margraf, L.R., Finegold, M.J., Weinberg, A.G., Rogers, B.B., 2000. Cytomegalovirus and human herpesvirus 6, but not human papillomavirus, are present in neonatal giant cell hepatitis and extrahepatic biliary atresia. Pediatr. Dev. Pathol. 3 (4), 367–373.

Drut, R., Drut, R.M., Gomez, M.A., Cueto Rua, E., Lojo, M.M., 2008. Presence of human papillomavirus in biliary atresia. J. Pediatr. Gastroenterol. Nutr. 27 (5), 530–535.

Estes, M.K., Graham, D.Y., Gerba, C.P., Smith, E.M., 1979. A plaque assay for the simian rotavirus SA11. J. Gen. Virol. 43 (3), 513–519.

Fickert, P., Stoger, U., Fuchsbichler, A., Moustafa, T., Marchall, H.U., Weiglein, A., Tsybrovskyy, O., Jaeschke, H., Zatloukal, K., Denk, H., Trauner, M., 2007. A new xenobiotic-induced mouse model of sclerosing cholangitis and biliary fibrosis. Am. J. Pathol. 171 (2), 525–536.

Fickert, P., Theuringer, A., Moustafa, T., Silbert, D., Gumhold, J., Tsybrovskyy, O., Lebofsky, M., Jaeschke, H., Denk, H., Trauner, M., 2010. The role of osteopontin and tumor necrosis factor alpha receptor-1 in xenobiotic-induced cholangitis and biliary fibrosis in mice. Lab. Invest. 90 (6), 844–852.

Glaser, S., Wang, M., Ueno, Y., Venter, J., Wang, K., Chen, H., Alpini, G., Holterman, A., 2010. Differential transcriptional characteristics of small and large biliary epithelial cells derived from small and large bile ducts. Am. J. Physiol. Gastrointest. Liver Physiol. 299 (3), G769–G777.

Groene, W.S., Shaw, R.D., 1992. Psoralen preparation of antigenically intact non-infectious rotavirus particles. J. Virol. Methods 38, 93.

Harada, K., Ozaki, S., Sudo, Y., Tsuneyama, K., Ohta, H., Nakanuma, Y., 2003. Osteopontin is involved in the formation of epithelioid granuloma and bile duct injury in primary biliary cirrhosis. Pathol. Int. 53, 8–17.

Huang, L., Wei, M.F., Feng, J.X., 2008. Abnormal activation of OPN inflammation pathway in livers of children with biliary atresia and relationship to hepatic fibrosis. Eur. J. Pediatr. Surg. 18, 224–229.

Jafri, M., Donnelly, B., Bondoc, A., Allen, S., Tiao, G., 2009. Cholangiocyte secretion of chemokines in experimental biliary atresia. J. Pediatr. Surg. 44, 500–507.

Kalica, A.R., James, H.D., Kapikian, A.Z., 1978. Hemagglutination by simian rotavirus. J. Clin. Microbiol. 7 (3), 314–315.

Li, X., O'Regan, A.W., Berman, J.S., 2003a. IFN-gamma induction of osteopontin expression in human monocytoid cells. J. Interferon Cytokine Res. 23 (5), 259–265.

Li, Z., Yang, S., Lin, H., Huang, J., Watkins, P.A., Moser, A.B., Desimone, C., Song, X.Y., Diehl, A.M., 2003b. Probiotics and antibodies to TNF inhibit inflammatory activity and improve nonalcoholic fatty liver disease. Hepatology 37 (2), 343–350.

Lorena, D., Darby, I.A., Gadeau, A.P., Leen, L.L., Rittling, S., Porto, L.C., Rosenbaum, J., Desmouliere, A., 2006. Osteopontin expression in normal and fibrotic liver; altered liver healing in osteopontin-deficient mice. J. Hepatol. 44 (2), 383–390.

Mack, C.L., Tucker, R.M., Sokol, R.J., Kotzin, B.L., 2005. Armed CD4+ Th1 effector cells and activated macrophages participate in bile duct injury in murine biliary atresia. Clin. Immunol. 115, 200–209.

Mack, C.L., Tucker, R.M., Lu, B.R., Sokol, R.J., Fontenot, A.P., Ueno, Y., Gill, R.G., 2006. Cellular and humoral autoimmunity directed at bile duct epithelia in murine biliary atresia. Hepatology 44 (5), 1231–1239.

Mahjoub, F., Shahsiah, R., Ardalan, F.A., Iravanloo, G., Sani, M.N., Zarei, A., Monajemzadeh, M., Farahmand, F., Mamishi, S., 2008. Detection of Epstein Barr virus by chromogenic in situ hybridization in cases of extra-hepatic biliary atresia. Diagn. Pathol. 3, 19.

Mano, Y., Ishii, M., Kisara, N., Kobayashi, Y., Ueno, Y., Kobayashi, K., Hamada, H., Toyota, T., 1998. Duct formation by immortalized mouse cholangiocytes: an in vitro model for cholangiopathies. Lab. Invest. 78, 1467–1468.

Mohanty, S.K., Ivantes, C.A.P., Mourya, R., Pacheco, C., Bezerra, J., 2010. Macrophages are targeted by rotavirus in experimental biliary atresia and induce neutrophil chemotaxis by Mip2/Cxcl2. Pediatr. Res. 67 (4), 345–351.

Nadler, E.P., Patterson, D., Violette, S., Weinreb, P., Lewis, M., Magid, M.S., Greco, M.A., 2009. Integrin alphavbeta6 and mediators of extracellular matrix deposition are up-regulated in experimental biliary atresia. J. Surg. Res. 154 (1), 21–29.

Nakai, A., Imano, M., Takeyama, Y., Shiozaki, H., Ohyanagi, H., 2008. An immunohistochemical study of osteopontin in hepatolithiasis. J. Hepatobiliary Pancreat. Surg. 15, 615–621.

Petersen, C., Biermanns, D., Kuske, M., Schakel, K., Meyer-Junghanel, L., Mildenberger, H., 1997. New aspects in a murine model for extrahepatic biliary atresia. J. Pediatr. Surg. 32 (8), 1190–1195.

Qiao, H., Zhaori, G., Jiang, Z., Chen, Y., Chen, Y., Hou, D., 1999. Detection of group C rotavirus antigen in bile duct and liver tissues of an infant with extrahepatic biliary atresia. Chin. Med. J. 112 (1), 93–95.

Racanelli, V., Rehermann, B., 2006. The liver as an immunological organ. Hepatology 42 (2), S54–S62.

Reed, L.J., Muench, H., 1938. A simple method of estimating fifty per cent endpoint. Am. J. Hyg. 27, 493.

Riepenhoff-Talty, M., Schaekel, K., Clark, H.F., Mueller, W., Uhnoo, I., Rossi, T., Fisher, J., Ogra, P.L., 1993. Group A rotaviruses produce extrahepatic biliary atresia in orally inoculated newborn mice. Pediatr. Res. 33 (4 Pt.1), 394–399.

Riepenhoff-Talty, M., Gouvea, V., Evans, M.J., Svensson, L., Hoffenberg, E., Sokol, R.J., Uhnoo, I., Greenberg, S.J., Schakel, K., Zhaori, G., Fitzgerald, J., Chong, S., el-Yousef, M., Nemeth, A., Brown, M., Piccoli, D., Hyams, J., Ruffin, D., Rossi, T., 1996. Detection of group C rotavirus in infants with extrahepatic biliary atresia. J. Infect. Dis. 174 (1), 8–15.

Rollo, E.E., Hempson, S.J., Bansal, A., Tsao, E., Habib, I., Rittling, S.R., Denhardt, D.L., Mackow, E.R., Shaw, R.D., 2005. The cytokine osteopontin modulates the severity of rotavirus diarrhea. J. Virol. 79 (6), 3509–3516.

Sahai, A., Malladi, P., Melin-Aldana, H., Green, R.M., Whitington, P.F., 2004. Upregulation of osteopontin expression is involved in the development of nonalcoholic steatohepatitis in a dietary murine model. Am. J. Physiol. Gastrointest. Liver Physiol. 287, G264–G273.

Shaw, R.D., Hempson, S.J., Mackow, E.R., 1995. Rotavirus diarrhea is caused by nonreplicating viral particles. J. Virol. 69 (10), 5946–5950.

Shivakumar, P., Campbell, K.M., Sabla, G.E., Miethke, A., Tiao, G., McNeal, M.M., Ward, R.L., Bezerra, J.A., 2004. Obstruction of extrahepatic bile ducts by lymphocytes is regulated by IFN-gamma in experimental biliary atresia. J. Clin. Invest. 114 (3), 322–329.

Sokol, R.J., Shepherd, R.W., Superina, R., Bezerra, J.A., Robuck, P., Hoofnagle, J.H., 2007. Screening and outcomes in biliary atresia: summary of a National Institutes of Health workshop. Hepatology 46 (2), 566–581.

Sun, J., Xu, Y., Dai, Z., Sun, Y., 2009. Intermittent high glucose enhances proliferation of vascular smooth muscle cells by upregulating osteopontin. Mol. Cell. Endocrinol. 313 (1–2), 64–69.

Syn, W.K., Choi, S.S., Liaskou, E., Karaca, G.F., Agboola, K.M., Oo, Y.H., Mi, Z., Pereira, T.A., Zdanowicz, M., Malladi, P., Chen, Y., Moylan, C., Jung, Y., Bhattacharya, S.D., Teaberry, V., Omenetti, A., Abdelmalek, M.F., Guy, C.D., Adams, D.H., Kuo, P.C., Michelotti, G.A., Whitington, P.F., Diehl, A.M., 2010. Osteopontin is induced by hedgehog pathway activation and promotes fibrosis progression in nonalcoholic steatohepatitis. Hepatology 53 (1), 106–115.

Szalay, G., Sauter, M., Haberland, M., Zuegel, U., Steinmeyer, A., Kandolf, R., Klingel, K., 2009. Osteopontin: a fibrosis-related marker molecule in cardiac remodeling of enterovirus myocarditis in the susceptible host. Circ. Res. 104, 851–859.

Tyler, K.L., Sokol, R.J., Oberhaus, S.M., Le, M., Karrer, F.M., Narkewicz, M.R., Tyson, R.W., Murphy, J.R., Low, R., Brown, W.R., 1998. Detection of reovirus RNA in hepatobiliary tissues from patients with extrahepatic biliary atresia and choledochal cysts. Hepatology 27 (6), 1475–1482.

Vetrone, S.A., Montecino-Rodriguez, E., Kudryashova, E., Kramerova, I., Hoffman, E.P., Liu, S.D., Miceli, M.C., Spencer, M.J., 2009. Osteopontin promotes fibrosis in dystrophic mouse muscle by modulating immune cell subsets and intramuscular TGF-β. J. Clin. Invest. 119, 1583–1594.

Whitington, P.F., Malladi, P., Melin-Aldana, H., Azzam, R., Mack, C.L., Sahai, A., 2005. Expression of osteopontin correlates with portal biliary proliferation and fibrosis in biliary atresia. Pediatr. Res. 57 (6), 837–844.

Zhang, M., Zeng, C.Q., Morris, A.P., Estes, M.K., 2000. A functional NSP4 enterotoxin peptide secreted from rotavirus-infected cells. J. Virol. 74 (24), 11663–11670.